

Silver(I)-Catalyzed Insertion of Carbene into Alkane C–H Bonds and the Origin of the Special Challenge of Methane Activation Using DFT as a Mechanistic Probe

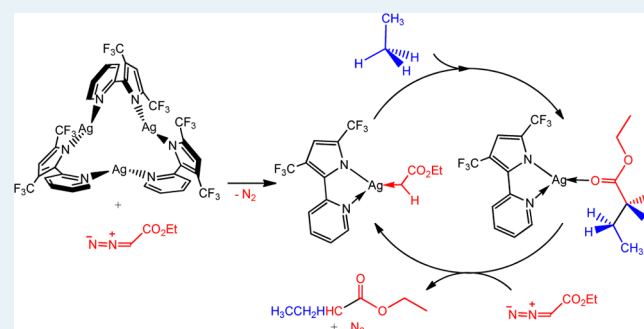
Jaime A. Flores, Nobuyuki Komine, Kuntal Pal, Balazs Pinter, Maren Pink, Chun-Hsing Chen, Kenneth G. Caulton,* and Daniel J. Mindiola*

Department of Chemistry and Molecular Structure Center, Indiana University, Bloomington, Indiana 47405, United States

Supporting Information

ABSTRACT: The argentate trinuclear cluster $\text{Ag}_3(\mu_2\text{-}3,5\text{-(CF}_3)_2\text{PyrPy})_3$ ($3,5\text{-(CF}_3)_2\text{PyrPy} = 2,2'\text{-pyridylpyrrolide}^-$ ligand) catalytically promotes the insertion of the carbene of ethyl diazoacetate at room temperature into the C–H bond of a series of alkanes ranging from ethane to hexane, as well as branched and cyclic hydrocarbons. In addition to experimental studies, we also present theoretical studies elucidating the mechanism to C–H activation and functionalization by the transient silver carbene monomer $(3,5\text{-(CF}_3)_2\text{PyrPy})\text{Ag}(\text{CHCO}_2\text{Et})$. On the basis of DFT studies, formation of the silver carbene complex was found to be rate-determining for alkane substrates such as ethane and propane. On the other hand, DFT studies on methane, a substrate that we failed to activate, revealed that carbene insertion into the C–H bond was overall rate-determining. Theoretical analysis of charge flow also shows that the change from separated reagents to the TS involves charge flow from alkane to the silver carbene carbon with the bridging H behaving as a conduit. KIE studies using cyclohexane as a substrate suggest that the product-determining step involves only modest C–H bond lengthening, which can be also represented as a very early transition state with respect to C–H insertion of the carbene.

KEYWORDS: silver, catalysis, carbene, pyridylpyrrolide



INTRODUCTION

Since the seminal discovery that metal-promoted carbenes can insert into aliphatic C–H bonds,¹ this branch of chemistry^{1–4} has bloomed over the past three decades, ultimately resulting in the development of potent catalysts that can functionalize C–H bonds in a stereoselective fashion^{5–15} as well as insert into volatile alkanes^{16–31} including methane.¹⁶ In the latter regard, other groups have successfully developed some metal catalysts that readily insert carbenes from ethyl diazoacetate (EDA) into aliphatic C–H bonds.^{16–31} More recently, halogen-rich variants of the tris-pyrazolyl borate (Tp) ligand have proven instrumental for the synthesis of silver catalysts, and these are the only systems known to convert volatile alkanes such as methane and ethane into the corresponding ester; supercritical conditions employed CO_2 solvent (Figure 1).¹⁶ This transformation is particularly attractive, since it allows for conversion of a C_1 feedstock such as methane (also a potent greenhouse gas approximately 23 times stronger than CO_2) into an ester that is widely used as an additive in glues, nail polish, as a highly polar solvent, and in gastroenterology for topical gallstone dissolution.³²

With the rise of anthropogenic methane in our earth's atmosphere since the late 1990s, alternative uses to burning of this greenhouse gas appeal both from an ecological and

industrial standpoint. It is estimated that flare stacks account for more than 31 billion dollars in loss from the burning of the most volatile of alkanes in natural gas.^{33,34} In the case of the second most abundant component in natural gas, ethane, the corresponding ester, ethyl butanoate (or ethyl butyrate) is widely used in flavoring or perfumery products and as a plasticizer for cellulose.^{35,36} As an alternative to combustion, the conversion of volatile alkanes into common chemicals of importance to industry is a paradigm, especially if these transformations could be performed catalytically and under mild conditions while involving the creation of a C–C bond. Likewise, understanding how a well-defined catalyst both activates and functionalizes alkane C–H bonds would constitute an important study, since it would allow for subsequent optimization of reaction conditions.

Dias and co-workers^{26,37–42} have described the use of Bi-CF_3 -substituted Tp (Figure 2) complexes of Ag and Cu, and Perez has described the bromo Tp analogs to carry out these C–H functionalizations. Further developments have included use of N-heterocyclic carbene (NHC) ligands on Ag and Au,

Received: April 19, 2012

Revised: August 5, 2012

Published: August 6, 2012

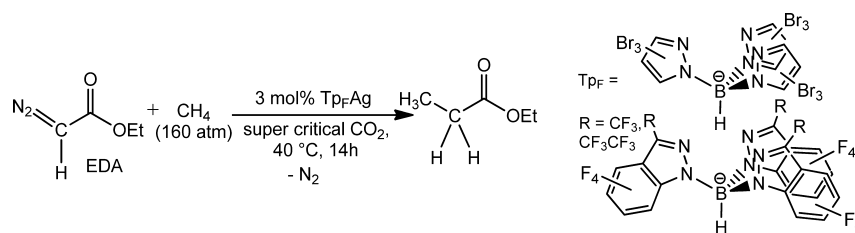


Figure 1. Catalytic C–H insertion of carbene into methane and ethane via TpAg complexes.

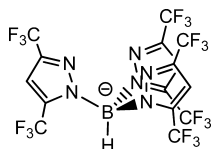


Figure 2. Tp ligand often used in catalytic C–H insertion reactions.

with finally success in detecting insertion into primary as well as secondary C–H bonds with these catalysts.

Regarding electrophilicity of the metal catalysts, it has been shown that a good correlation exists between increasing catalytic activity of TpM and a higher ν_{CO} of the corresponding TpM(CO) complex. TpBr³Cu(CO) is reported³⁹ to have a stretching frequency of 2073 cm⁻¹, and (PyrPy)Cu(CO) has a frequency of 2106 cm⁻¹. In the case of pyridylpyrrolide,⁴³ the value for the silver complex lies 19 cm⁻¹ higher than that for copper, again consistent with electrophilicity being central to alkane C–H insertions. Consistent with this, a combined computational and spectroscopic study concluded that the copper-olefin linkage is mainly sustained by σ -donation, lacking a substantial degree of π -back-donation.⁴⁴ The most highly fluorinated copper and silver species, based on tris-indazolyborate, show the highest CO stretching frequencies and gives correspondingly high alkane insertion catalysis performance; the more reactive silver catalyst also showed some insertion into the more challenging primary C–H bonds.²⁰

All of the previous work has been performed with tridentate ligands except one case,⁴⁵ in which catalysis employed a bis-oxazoline ligand on Ag to prove transfer of chirality (used only for the CH₂Cl₂ substrate), but the mechanism with this bidentate ligand was not investigated. We report herein an easy-to-prepare air- and water-stable silver(I) catalyst, in the resting state of a trinuclear complex supported by a bidentate ligand,⁴³ that can promote the insertion of the carbene moiety of EDA, N₂CH(CO₂Et), in some cases regioselectively, into cyclic, linear, and branched alkanes, all under mild conditions and without need for slow addition of EDA under diluted conditions. For most hydrocarbons, and in accord with previous work in this area,^{3,10,17,20,21,23,24,26,31,37,38,40–42} insertion of the carbene is selective for the 2° carbon. We also demonstrate this catalyst to convert volatile alkanes such as ethane, propane, and butane into the corresponding ester when combined with EDA. Analysis of the mechanism by DFT using various alkanes as substrates suggests a silver monomer to be the active form of the catalyst, involving a concerted C–H insertion step taking place at an electrophilic carbene carbon and where the alkane H atom serves as a conduit for charge flow. The metal is not directly involved in the C–H bond activation step but serves as a delivery vehicle of the EDA-derived carbene.

EXPERIMENTAL DETAILS

General Considerations. All manipulations were carried out in air (unless otherwise stated). NMR spectra were recorded in CDCl₃ or CD₂Cl₂ at 25 °C on Varian Inova-400 and -500 spectrometers (¹H, 400.11 MHz; ¹⁹F, 376.48 MHz; ¹³C, 125.68 MHz). Proton and carbon chemical shifts are reported in parts per million versus Me₄Si (0.0 ppm). High-resolution mass spectra were obtained on a ThermoFinnigan MAT95XP mass spectrometer with a Thermo Electron trace gas chromatograph. Ethyl diazoacetate (85% in CH₂Cl₂), Ag₂O, alkanes (methane, ethane, propane, butane, *n*-pentane, cyclopentane, *n*-hexane, cyclohexane, cyclohexane-*d*₁₂, 2-methylbutane, 2,3-dimethylbutane), C₆F₆, CDCl₃, and CD₂Cl₂ were purchased from commercial sources and used as received. H(3,5-(CF₃)₂PyrPy) was synthesized following a published procedure.⁴⁶

Synthesis of Complex Ag₃(μ -3,5-(CF₃)₂PyrPy)₃ (1). H(3,5-(CF₃)₂PyrPy) (0.3232 g, 1.154 mmol) and Ag₂O (0.2849 g, 1.229 mmol) were stirred in acetonitrile (45 mL) at room temperature overnight and without protection from light. The mixture was then filtered through a short plug of Celite, and the solvent from the filtrate was removed under vacuum. The residue was dissolved in benzene (2 mL) and pumped dry to ensure complete removal of acetonitrile. A nearly colorless powder was obtained. Yield: 98%. mp: 165 °C (darkens), >250 °C (decomp). ¹H NMR (25 °C, C₆D₆): δ 7.19 (br, 1H), 6.88 (s, 1H), 6.86 (s, 1H), 6.60 (t, ³J_{HH} = 6.6 Hz, 1H), 6.09 (br, 1H). ¹⁹F NMR (25 °C, C₆D₆): δ 52.91 (s, 3F), 59.42 and 59.96 (overlapped br, 3F). MS (MALDI, negative): exptl. 366.64 [¹⁰⁷AgL–F]⁻, C₁₁H₅¹⁰⁷AgF₃N₂, calcd. 366.94; exptl. 368.64 [¹⁰⁹AgL–F]⁻, C₁₁H₅¹⁰⁹AgF₃N₂, calcd. 368.94; exptl. 385.67 [¹⁰⁷AgL]⁻, C₁₁H₅¹⁰⁷AgF₆N₂, calcd. 385.94; exptl. 387.66 [¹⁰⁹AgL]⁻, C₁₁H₅¹⁰⁹AgF₆N₂, calcd. 387.94.

Silver(I)-Catalyzed Insertion of Carbene of Ethyl Diazoacetate into Liquid Alkane C–H Bonds. In a vial protected from light using black tape, the silver catalyst (5 mg, based on monomer Ag(3,5-(CF₃)₂PyrPy) (1), 0.013 mmol) was dissolved in solvent and alkane under air. The mixture was stirred vigorously for several minutes, and then EDA (32 μ L, 0.26 mmol) was added with a syringe all at once, at room temperature. The mixture was allowed to stir at 25 °C for 3 days. A weighed amount of 1,3,5-tribromobenzene was added to the reaction mixture, and the crude products were analyzed by ¹H NMR spectroscopy in CDCl₃. Spectral data of the products were compared with those in the literature. The product yields were calculated from ¹H NMR integral of the spectra for the methylene protons of the CH₂CO₂Et fragments. Yield of products and amount of unreacted EDA are quoted as an average of at least two experiments.

Silver(I)-Catalyzed Insertion of Carbene of Ethyl Diazoacetate into Gaseous Alkane C–H Bonds. Reactions involving the activation of ethane were performed in closed 25

mL stainless steel autoclave reaction vessels. Cylindrical 25 mL glass liners equipped with small Teflon stir-bars were used for all experiments. Typically, the vessel was initially charged with Ag complex **1** (5 mg, 0.013 mmol as monomer) and solvent (3 mL) under air. The vessel was sealed and connected to an ethane-pressurized stainless-steel transfer line and was then pressurized to the desired pressure (100, 200, 300, 400, 500, and 600 psi). The mixture was allowed to stir at 25 °C for 3 days, then the vessel was carefully depressurized. The reaction solutions were transferred into vials, and 1,3,5-tribromobenzene was added to the reaction mixture. The crude products were analyzed by ¹H NMR spectroscopy. Spectral data of the products were compared with those in the literature. The product yields were calculated from ¹H NMR integral of the methylene protons of the CH₂CO₂Et fragments. Yield of products and amount of unreacted EDA are quoted as an average of at least two experiments.

Silver(I)-Catalyzed Insertion of Carbene into Cyclopentane C–H Bonds in the Presence of Water. The silver catalyst **1** (5 mg, 0.013 mmol as monomer) was dissolved in a mixture of CD₂Cl₂ (1 mL) and cyclopentane (1 mL). After addition of water (0.2–30 μL), the mixture was allowed to stir for 5 min, then EDA (32 μL, 0.26 mmol) was added with a syringe at once at 25 °C and in the absence of light. After 2 days, 1,3,5-tribromobenzene was added to the reaction mixture, and the crude products were analyzed by ¹H NMR spectroscopy in CDCl₃. The products yields were calculated from the ¹H NMR integral of the spectra for the methylene protons of the CH₂CO₂Et fragments. The results are summarized in Table S2 of the Supporting Information.

KIE Experiments. The silver catalyst **1** (5 mg, 0.013 mmol as monomer) was dissolved in CD₂Cl₂ or C₆F₆ (1 mL), cyclohexane (0.5 mL, 4.63 mmol), and cyclohexane-*d*₁₂ (99.8% D, 0.5 mL, 4.63 mmol), then EDA (32 μL, 0.26 mmol) was added with a syringe all at once, at 25 °C, and in the absence of light. After 1 day, 1,3,5-tribromobenzene was added to the reaction mixture. The crude products were analyzed by ¹H NMR spectroscopy in CDCl₃. The product yields and ratio were calculated from the ¹H NMR integral of the methylene protons of the CH₂CO₂Et and CHDCO₂Et fragments. The KIE value (*k*_H/*k*_D) was calculated from the yields of the C–H insertion products. The results are summarized in Table S3 of the Supporting Information.

X-ray Crystallography Data Collection and Structure Refinement. A colorless plate of **1** (approximate dimensions 0.20 × 0.20 × 0.05 mm) was placed onto the tip of a 0.1 mm diameter glass capillary and mounted on a Bruker APEX II Kappa Duo diffractometer equipped with an APEX II detector at 150(2) K. The data collection was carried out using Mo Kα radiation (graphite monochromator) with a frame time of 20 s and a detector distance of 5.00 cm. A collection strategy was calculated, and complete data to a resolution of 0.70 Å with a redundancy of 4 were collected. Five major sections of frames were collected with 0.50° ω and φ scans. Data to a resolution of 0.77 Å were considered in the reduction. Final cell constants were calculated from the *xyz* centroids of 9944 strong reflections from the actual data collection after integration (SAINT).⁴⁷ The intensity data were corrected for absorption (SADABS).⁴⁸ The space group P1̄ was determined on the basis of the intensity statistics and the lack of systematic absences. The structure was solved using SIR-2004⁴⁹ and refined with SHELXL-97.⁵⁰ A direct-methods solution was calculated, which provided most non-hydrogen atoms from the E-map. Full-

matrix least-squares/difference Fourier cycles were performed, which located the remaining non-hydrogen atoms. All non-hydrogen atoms were refined with anisotropic displacement parameters. The hydrogen atoms were placed in ideal positions and refined as riding atoms with relative isotropic displacement parameters. The final full matrix least-squares refinement converged to *R*₁ = 0.0233 and *wR*₂ = 0.0479 (*F*², all data). The remaining electron density is miniscule and located on bonds. Crystal data and structure refinement for complex **1** are included in the Supporting Information.

■ COMPUTATIONAL DETAILS

All calculations were carried out using DFT as implemented in the Jaguar 7.7⁵¹ suite of ab initio quantum chemistry programs. Geometry optimizations were performed with the B3LYP^{52–55} functional and the 6-31G** basis set. Ag ions were represented using the Los Alamos LACVP basis^{56,57} that includes relativistic effective core potentials. The energies of the optimized structures were reevaluated by additional single-point calculations on each optimized geometry using Dunning's correlation consistent triple-ζ basis set⁵⁸ cc-pVTZ(-f), which includes a double set of polarization functions. For Ag, we used a modified version of LACVP, designated as LACV3P, in which the exponents were deconstructed to match the effective core potential with the triple-ζ quality basis set. Solvation energies were evaluated by a self-consistent reaction field^{59–61} (SCRF) approach based on accurate numerical solutions of the Poisson–Boltzmann equation. In the results reported, solvation calculations were carried out with the 6-31G**/LACVP basis at the optimized gas-phase geometry employing the dielectric constants of ε = 9.08, solvent = dichloromethane. Analytical vibrational frequencies within the harmonic approximation were computed with the 6-31G**/LACVP basis to confirm proper convergence to well-defined minima or saddle points on the potential energy surface. The energy components have been computed with the following protocol. The free energy in solution phase *G*(sol) has been calculated as follows:

$$G(\text{sol}) = G(\text{gas}) + G(\text{solv}) \quad (1)$$

$$G(\text{gas}) = H(\text{gas}) - TS(\text{gas}) \quad (2)$$

$$H(\text{gas}) = E(\text{SCF}) + \text{ZPE} \quad (3)$$

$$\Delta E(\text{SCF}) = \sum_{\text{for reactants}} E(\text{SCF}) \text{ for products} - \sum E(\text{SCF}) \quad (4)$$

$$\Delta G(\text{sol}) = \sum_{\text{for reactants}} G(\text{sol}) \text{ for products} - \sum G(\text{sol}) \quad (5)$$

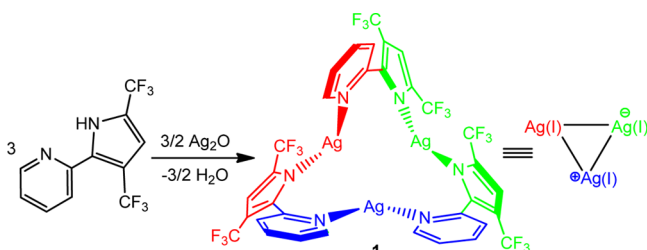
G(gas) is the free energy in gas phase; *G*(solv) is the free energy of solvation as computed using the continuum solvation model; *H*(gas) is the enthalpy in gas phase; *T* is the temperature (in K); *S*(gas) is the entropy in gas phase; *E*(SCF) is the self-consistent field energy (i.e. “raw” electronic energy as computed from the SCF procedure), and ZPE is the zero point energy. Note that by entropy here, we refer specifically to the vibrational/rotational/translational entropy of the solute(s); the entropy of the solvent is incorporated implicitly in the continuum solvation model. To locate transition states, the potential energy surface was first explored approximately using the linear synchronous transit (LST)⁶² method, followed by a quadratic synchronous transit (QST)⁶³

search using the LST geometry as an initial guess. IRC (intrinsic reaction coordinate) scans were performed to verify the convergence of the transition states to appropriate reactants and products.

RESULTS AND DISCUSSION

Synthesis and Characterization of Complex 1. We have previously shown that attachment of a cisoid 2,2'-pyridyl pyrrolide ligand (Scheme 1), 3,5-(CF₃)₂PyrPy⁻, to monovalent

Scheme 1. Synthesis of Complex 1 from Ag₂O and H(3,5-(CF₃)₂PyrPy)₃^a



^aThe different silver environments are illustrated with color.

copper and in the absence of an additional ligand/Lewis base source yields an unprecedented structure in which the pyridylpyrrolide twists internally to bridge two metals, thereby yielding a trinuclear complex, Cu₃(μ₂-3,5-(CF₃)₂PyrPy)₃.⁴³ Despite forming a trinuclear cluster, we view Cu₃(μ₂-3,5-(CF₃)₂PyrPy)₃ as a possible precursor to the unsaturated and reactive Cu(I) fragment Cu(3,5-(CF₃)₂PyrPy)^{43,64} when confronted by some substrate. We are interested in exploring the generality of this bridging and trimerization phenomenon for heavier coinage metals, since these have been demonstrated

to be the most reactive toward alkanes.¹⁶ Accordingly, the trinuclear complex Ag₃(μ₂-3,5-(CF₃)₂PyrPy)₃ (**1**)^{65–73} was synthesized readily from Ag₂O and the free ligand in NCCH₃ at 25 °C (Scheme 1).⁷⁴

The ¹⁹F NMR spectrum of **1** in CD₂Cl₂ or toluene-*d*₈ at room temperature displays signals in two regions, separated by ~7 ppm, but the higher field one (region A, -59.8 ppm) being broad (Δν_{1/2} = 450 Hz) compared with the sharp one at -52.8 ppm (region B). This suggests dynamic phenomena, and we propose a mechanism for this fluxionality below. A study of the ¹⁹F NMR spectrum between -50 and +25 °C is consistent with the molecule's being trinuclear with no symmetry relating the Ag(3,5-(CF₃)₂PyrPy) units (Scheme 1). At -25 °C, one observes two signals for both region A and for region B, but each has 1:2 intensities. At -50 °C, a total of six signals are displayed, as similarly observed for the copper analog.^{43,74} In the range -25 to +25 °C, the two signals in region A coalesce, and the two broad ones at -59 ppm (region B) finally coalesce into one above 25 °C, in accord with a barrier of ~13.9 kcal/mol (Figure 3). At higher temperature, the NMR spectral data is equally interesting, since coalescence of the 3 and 5 positions of CF₃ groups on the ligand (into two singlets) is observed at 50 °C and above (Figure 3). As a result, all our data is in accord with a diamagnetic trinuclear complex lacking any symmetry operation, but with fluxional site exchange rearrangement, which has a lower barrier than for Cu₃(μ₂-3,5-(CF₃)₂PyrPy)₃. The lack of spectral difference for **1** in CD₂Cl₂ vs *d*₈-toluene indicates that the arene does not coordinate to the metal.⁷⁴ Notably, solid complex **1** is both air- and light-stable at room temperature for several weeks; dichloromethane solutions are stable for at least 2 days in the presence of light (even in the presence of 100 equiv of water), as well as stable at high temperature in toluene for several hours (70–100 °C).

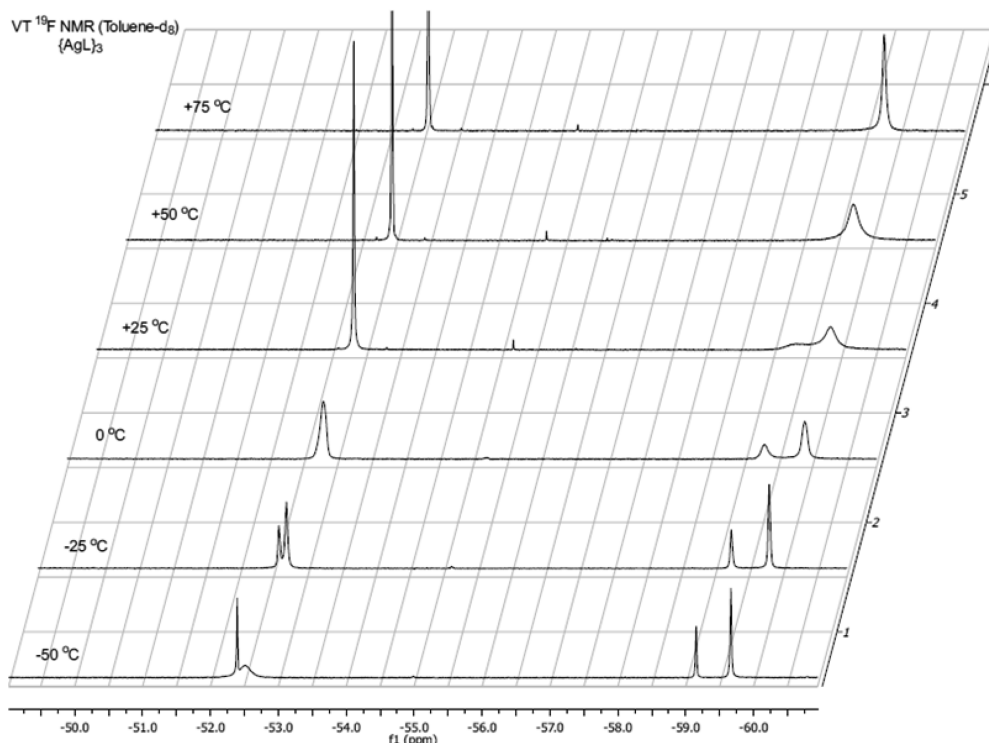


Figure 3. Stacked ¹⁹F NMR spectra for complex **1** ranging from -50 to +75 °C.

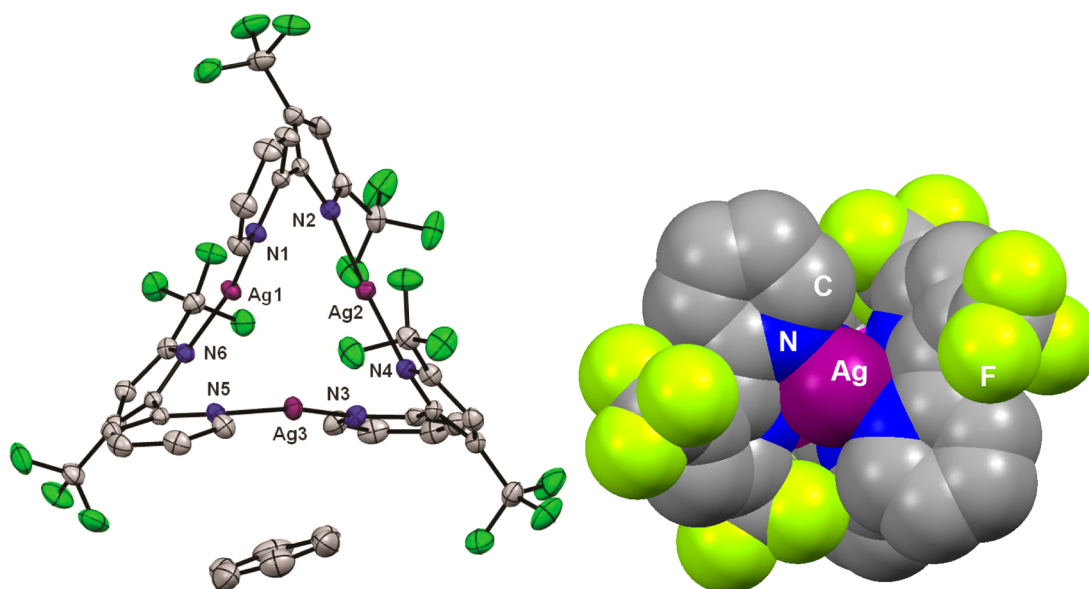
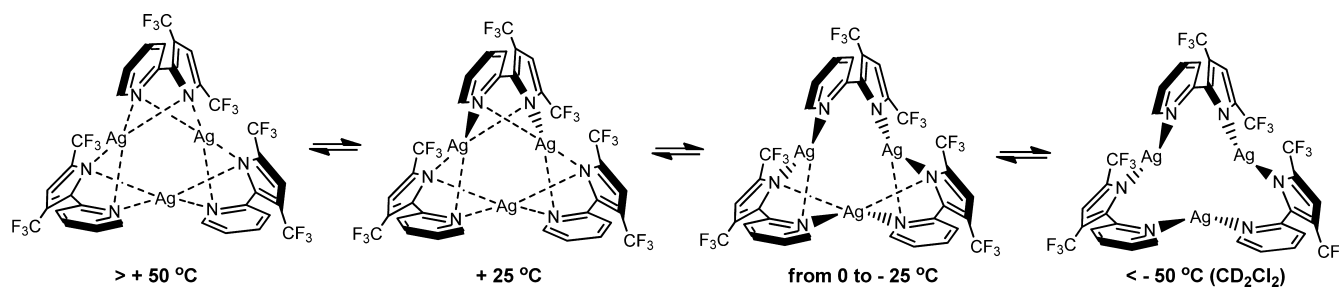
Scheme 2. Proposed Mechanism for Fluxional Behavior of Complex 1 Based on the Variable Temperature ^{19}F NMR Spectra

Figure 4. (left) Structural drawing (50% thermal ellipsoid probabilities) of the non-hydrogen atoms of $1 \cdot \text{C}_6\text{H}_6$ depicting selected atom labeling. Selected structural parameters reported with distances (Å) and angles ($^\circ$): Ag1–N6, 2.1251(18) Å; Ag1–N1, 2.1456(19); Ag1–Ag3, 2.9837(3); Ag1–Ag2, 3.0015(3); Ag2–N2, 2.0955(19); Ag2–N4, 2.1042(19); Ag2–Ag3, 3.0973(3); Ag3–N5, 2.1683(19); Ag3–N3, 2.177(2); N6–Ag1–N1, 163.06(7); Ag3–Ag1–Ag2, 62.328(7); N2–Ag2–N4, 176.70(7); Ag1–Ag2–Ag3, 58.554(6); N5–Ag3–N3, 165.01(7); Ag1–Ag3–Ag2, 59.118(6). (right) Space-filling model of **1** viewed from a direction where the lattice benzene binds and where substrate is proposed to approach. Hydrogen atoms have been omitted for clarity, and the Ag_3 plane lies horizontally in this view.

The dynamic process revealed by the ^{19}F NMR spectra collected between -50 and $+75$ $^\circ\text{C}$ may involve fast exchange of each N to bind rapidly to two Ag atoms, thus resulting in the observation of a broad signal. The role of the Ag^+ ion might be important to consider, since the more electron-deficient ion could undergo faster exchange of the pyrrolides-N more so than the silver neighbors. The same dynamic process should occur for the other two neighboring Ag ions, but at higher temperatures. Scheme 2 proposes how the exchange process shifts from a 1:1:1 ratio at low temperature (for inequivalent (3,5-(CF_3) $_2$ PyrPy) units) to a 1:2 ratio and, finally, to all ligands being equivalent. At this point, however, we cannot assign with certainty which of the three silver ions is doing the fluxionality more rapidly than the other two. Our proposed mechanism in Scheme 2 suggests the Ag^+ ion bound to two pyridine moieties to be the initial site for exchange since these sites are expected to be more labile.


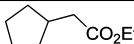
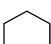
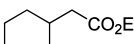

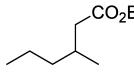
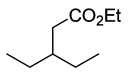
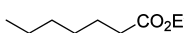
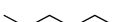
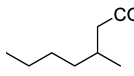
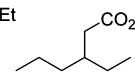

Crystals of **1** were grown from benzene and were used for a single-crystal X-ray diffraction structure determination (Figure 4). As deduced from the NMR spectroscopic data, the structure showed a non- C_3 symmetric trinuclear species analogous to, but not crystallographically isomorphous with, that of the copper analog.⁴³ As shown in Scheme 1, one silver binds two pyridyl donors of the ligand (hence, it is a formal cationic center, blue),

and the second has two pyrrolide donors of the ligand (hence, an anion, green), and the third silver has one pyridyl and one pyrrolide motif of each ligand (hence, neutral, red). The Ag/Ag distances, 2.9837(3)–3.0973(3) Å, give no support for any bond and are ~ 0.3 Å longer than those observed for the copper analog.

Density functional theory calculations show only small Wiberg bond orders.⁷⁴ While the copper analog has evidence for pyrrolide nitrogens *bridging* to the cationic copper, these analogous secondary $\text{Ag}\cdots\text{N}$ distances are > 2.77 Å, suggesting no bridging interactions. As a result, angles N–M–N are closer to linear for Ag (163.1–176.7 $^\circ$) than for Cu (157.5–171.4 $^\circ$). This structure also reveals the ability of the pyridylpyrrolide ligand to twist by 37–47 $^\circ$ around the inter-ring C–C bond. Complex **1** cocrystallizes with one benzene molecule in the crystal lattice, which π stacks with one pyridyl ring, with the closest C/C distance being 3.62 Å (Figure 4).⁷⁴

In contrast to the copper structure,⁴³ the expansion of the metal/metal distances render the silver centers more accessible to external reagents. This is evident not only from a space-filling drawing (Figure 4), but also from the fact that the benzene in the unit cell shows two contacts from two adjacent carbons to the cationic $\text{Ag}(3)$ center at 3.00 and 3.24 Å.⁷⁴ Since this silver is the one that is formally cationic⁷⁴ and, thus, the

Table 1. Catalytic Carbene Insertion into C–H Bonds with Ag(I).^a

		$\text{R-H} \xrightarrow[\text{CH}_2\text{Cl}_2 \text{ (or } \text{C}_6\text{F}_6\text{), EDA (N}_2\text{CHCO}_2\text{Et), -N}_2]{\text{5 mol \% of Ag(3,5-(CF}_3\text{)}_2\text{PyrPy) as monomer}} \text{R-CHHCO}_2\text{Et}$						
Substrate	Solvent	Time/ day	Product(s)	%CH insertion products (ratio)	% of dimers		%Un reacted EDA	
					(Z)	(E)		
1		CD ₂ Cl ₂	2		84	1	1	0
2		C ₆ F ₆	2		94	1	3	0
3		CDCl ₃	2		21	0	0	86
4		CCl ₄	2		13	0	0	79
5		ClCH ₂ CH ₂ Cl	7		33	1	0	21
6 ^b		CD ₂ Cl ₂	2		79	1	2	0
7		CD ₂ Cl ₂	3		88	1	2	0
8		C ₆ F ₆	3		68	1	2	0
9		CD ₂ Cl ₂	3	  	33 (8:2:1)	2	3	33
10 ^c		CD ₂ Cl ₂	3		38 (4:2:1)	1	2	20
11		C ₆ F ₆	3		47 (5:2:1)	2	4	0
12 ^c		C ₆ F ₆	3		51 (6:2:1)	1	2	0
13		CD ₂ Cl ₂	3	  	41 (5:2:1)	2	3	21
14 ^c		CD ₂ Cl ₂	3		40 (7:3:1)	1	2	15
15		C ₆ F ₆	3		48 (5:2:1)	2	3	0
16 ^c		C ₆ F ₆	3		55 (5:2:1)	1	2	0

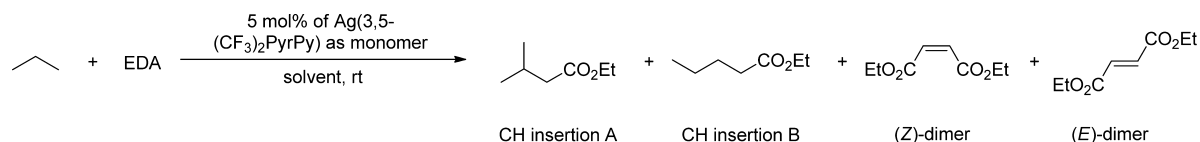
^aReaction conditions: Based on monomer Ag(3,5-(CF₃)₂PyrPy) (0.013 mmol), EDA (0.26 mmol), alkane substrate (1 mL), solvent (1 mL), 25 °C, in the dark. ^bUnder light. ^cAlkane substrate (2 mL).

most electrophilic silver in the trinuclear core, this may indicate that this solid state association with benzene has more than a steric, “hole filling”, origin; that would speak for higher solution phase reactivity at this silver toward arriving reagents.

Catalytic Activity of Complex 1. Treatment of complex 1 under catalytic conditions (5 mol % of Ag) with EDA and cyclopentane in CD₂Cl₂ forms the ester ethyl cyclopentyl acetate in 84% yield with minimal production of the undesired (*E*)- and (*Z*)-carbene dimers fumarate and maleate, respectively (entry 1, Table 1). The products from all catalytic reactions were analyzed by a combination of ¹H NMR spectroscopy and GC/MS. Yields are based not on isolation but on ¹H NMR

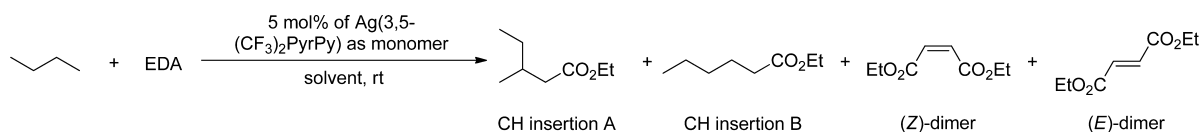
spectroscopy for several runs using the integral of the methylene protons of the CH₂CO₂Et fragment. We observe negligible product of insertion into solvent C–Cl bond.⁷⁵ Using 2–10 mol % of catalyst resulted in the best yields; smaller amounts (<1 mol %) of 1 did not fully convert the excess EDA.

Variation of the solvent medium revealed that C₆F₆ improved the yield of ethyl cyclopentyl acetate to 94% (entry 2, Table 1), whereas other chlorinated solvents such as CHCl₃, CCl₄, and ClCH₂CH₂Cl lowered the yield; in some cases, significantly (entries 3–5, Table 1). Notably, the presence of trace water (0.022 mmol) lowered the yield of ethyl cyclopentyl acetate

Table 2. Catalytic Carbene Insertion into C–H Bonds of Propane with Ag(I)^a

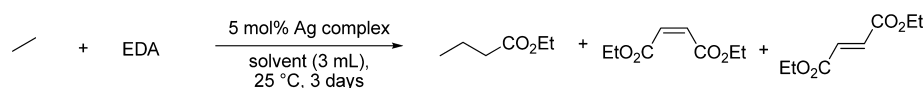
	amt of propane		solvent	time/days	% of CH insertion products	ratio % of products		% of dimers		% un reacted EDA
	mol	eq to EDA				A	B	(Z)	(E)	
1	0.15	591	CD ₂ Cl ₂	1	19	83	17	1	2	52
2	0.24	931	CD ₂ Cl ₂	1	51	83	17	2	3	31
3	0.23	893	CD ₂ Cl ₂	3	35	83	17	3	4	35
4	0.40	1544	CD ₂ Cl ₂	3	33	84	16	4	5	27
5	0.18	694	C ₆ F ₆	3	36.5	84	16	1	2	20
6	0.33	1293	C ₆ F ₆	3	37.4	83	17	5	9	20

^aReaction conditions: based on monomer Ag(3,5-(CF₃)₂PyrPy) (0.013 mmol), EDA (0.26 mmol), solvent (3 mL), 25 °C, in the dark.

Table 3. Catalytic Carbene Insertion into C–H Bonds of Butane with Ag(I)^a

	amt of butane		solvent	time/days	% of CH insertion products	ratio % of products		% of dimers		unreacted EDA/%
	mol	eq to EDA				A	B	(Z)	(E)	
1	0.16	618	CD ₂ Cl ₂	1	52	85	15	1	2	44
2	0.11	413	CD ₂ Cl ₂	3	65	85	15	1	2	18
3	0.13	496	CD ₂ Cl ₂	3	66	85	15	2	3	5
4	0.16	599	CD ₂ Cl ₂	3	43	86	14	2	3	19
5	0.11	411	C ₆ F ₆	3	36	77	23	1	3	45
6	0.12	477	C ₆ F ₆	3	42	91	9	1	2	17

^aReaction conditions: Based on monomer Ag(3,5-(CF₃)₂PyrPy) (0.013 mmol), EDA (0.26 mmol), solvent (3 mL), 25 °C, for 3 days, in the dark.

Table 4. Catalytic Carbene Insertion into C–H Bonds of Ethane with Ag(I)^a

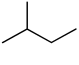
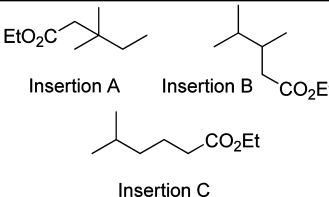
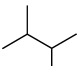
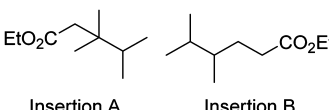
entry	solvent	pressure/psi	yield % of CH insertion product	yield % of dimers		unreacted EDA/%
				(Z)	(E)	
1	CD ₂ Cl ₂	100	4	5	9	0
2	CD ₂ Cl ₂	200	11	3	6	4
3	CD ₂ Cl ₂	300	13	3	6	8
4	CD ₂ Cl ₂	400	17	2	5	17
5	CD ₂ Cl ₂	500	8	4	7	48
6	CD ₂ Cl ₂	600	8	9	13	20
7	C ₆ F ₆	100	11	4	7	8
8	C ₆ F ₆	200	11	6	9	13
9	C ₆ F ₆	400	15	4	5	39
10	C ₆ F ₆	500	16	3	7	38
11	ClCH ₂ CH ₂ Cl	300	9	3	5	0

^aReaction conditions: based on monomer Ag(3,5-(CF₃)₂PyrPy), EDA (0.26 mmol), solvent (3 mL), 25 °C, for 3 days, in the dark.

only to 77%, but adding a larger amount of water to the reaction mixture (1.65 mmol) reduced the yield by half.⁷⁴ We observed no evidence for ethyl glycolate from hydration of EDA or the carbene.^{76,77} We propose that water inhibits the formation of a Ag(I)-EDA adduct, (3,5-(CF₃)₂PyrPy)Ag(EDA), via formation of a putative aqua complex (3,5-(CF₃)₂PyrPy)Ag(OH₂) (>100 equiv of water failed to produce

any products, on the basis of ¹H NMR spectroscopy, by competitive binding of the catalyst; see Table S5 of the Supporting Information). Likewise, performing the reaction in air or light with 5 mol % of **1** in CD₂Cl₂ did not lower the yield of ester formed from cyclopentane C–H carbene insertion.⁷⁴ Cyclohexane can also be functionalized cleanly to the corresponding ester in nearly quantitative yield (entry 7,

Table 5. Catalytic Carbene Insertion into Branched C–H Bonds with Ag(I).^a

Substrate (Amount)	Solvent	Product(s)	Total yield% of CH insertion products (ratio)	Yield% of Dimers		Un- reacted EDA/%							
				(Z)	(E)								
 1 (1 mL)	CD ₂ Cl ₂		13 (5:3:1)	1	1	67							
							2	(2 mL)	CD ₂ Cl ₂	18 (3:2:1)	1	2	53
							3	(1 mL)	C ₆ F ₆	41 (3:2:1)	2	3	0
							4	(2 mL)	C ₆ F ₆	42 (2:2:1)	1	2	0
 5 (1 mL)	CD ₂ Cl ₂		24 (5:1)	2	4	19							
							6	(2 mL)	CD ₂ Cl ₂	32 (6:1)	2	3	14
							7	(1 mL)	C ₆ F ₆	36 (5:1)	2	3	0
							8	(2 mL)	C ₆ F ₆	44 (7:1)	2	3	2

^aReaction conditions: based on monomer Ag(3,5-(CF₃)₂PyrPy) (0.013 mmol), EDA (0.26 mmol), alkane substrate, solvent (1 mL), 25 °C, for 3 days, in the dark.

Table 1). In the latter case, 5 or 10 mol % of catalyst provided similar yields (89%) over 1–2 days, but 0.5–2 mol % lowered the yield (<77%) and extended the time to completion to >6 days.⁷⁴ In this case, switching the solvent to C₆F₆ (using 5 mol % of **1**) lowered the yield of the ester to 68% (entry 8, Table 1).

Likewise, complex **1** also promotes the activation and functionalization of linear C₃ to C₆ alkanes. Tables 1–4 depict our optimized reaction conditions used with **1** and a series of linear alkanes. *n*-Pentane and *n*-hexane could be catalytically transformed, in ~50% yield and with 5 mol % of **1** in CD₂Cl₂, to the corresponding ester with preferential insertion of the carbene at the 2-position (insertion A), as opposed to insertion into the 3- (insertion B) and terminal positions (insertion C) (entry 10, Table 1). However, some formation of fumarate and maleate is observed (<5% combined) along with some unreacted EDA. The use of C₆F₆ did improve the yield (~47–55%, entries 12, 13, 16, and 17 in Table 1). In general, insertion into secondary C–H bonds is favored over primary, as is generally observed with other catalysts.^{3,17,20,21,23,24,26,31,37,38,40–42}

Volatile alkanes, such as butane, propane and ethane, can also be converted, catalytically by complex **1** in CD₂Cl₂ at room temperature over 3 days (Table 2 and 4). As shown in Tables 3 and 4, the yield of product resulting from carbene insertion into the secondary position in propane and butane is at least 5 times more than that of the terminal position. Propane can be also functionalized 5 times more selectively at the secondary position, as opposed to the primary (Table 2). However, formation of fumarate and maleate is slightly more evident because of lower alkane molarity, and the use of higher concentrations of the propane does not improve the yield of

ester products. Increasing the concentration of propane over 1 day did improve the yield of C–H insertion products, with the 2° C–H bond being preferred at least 5 times more (entries 1 and 2, Table 2). Allowing the reaction to proceed for 3 days did not improve the yield (entries 3 and 4, Table 2), and switching the solvent from CD₂Cl₂ to C₆F₆ resulted in a slight decrease in the yield (entries 5 and 6, Table 2). For the latter conditions, increasing the concentration of propane did not deviate yields from 36 to 37% (entry 6, Table 2), and selectivity was still preferred at the 2° C–H with a 5:1 ratio (C–H insertion A versus C–H insertion B, Table 2).

When butane is used as the substrate, ~51% yield of C–H insertion product is obtained, with a slight increase to ~65% when using higher concentrations of alkane (entries 2 and 3 in Table 3). However, increasing the alkane concentration can result in the observation of more unreacted EDA (entries 1 and 5, Table 3). Using C₆F₆ over CD₂Cl₂ does not improve the yield; instead, it lowers it to 30–40% (entries 5 and 6, Table 3). The selectivity for the 2° C–H group is preferred 10–5 times over the terminal position. Notably, slow addition of EDA via a controlled diffusion pump was not necessary, since we observed no significant formation of the carbene dimerization products.

Most notably, ethane can be converted to ethyl butanoate, reproducibly and catalytically, in yields ranging from 4 to 17% (without modest yield improvement and less EDA dimers with increasing pressure) along with concurrent formation of carbene coupled isomers (Table 4).⁷⁴ Varying the pressure of ethane (100–600 psi, entries 1–6, Table 4) or solvent medium (entries 7–11, Table 4) did not substantially improve the formation of the ester. These yields are comparable to Perez's recent results (40 °C and supercritical conditions with CO₂),

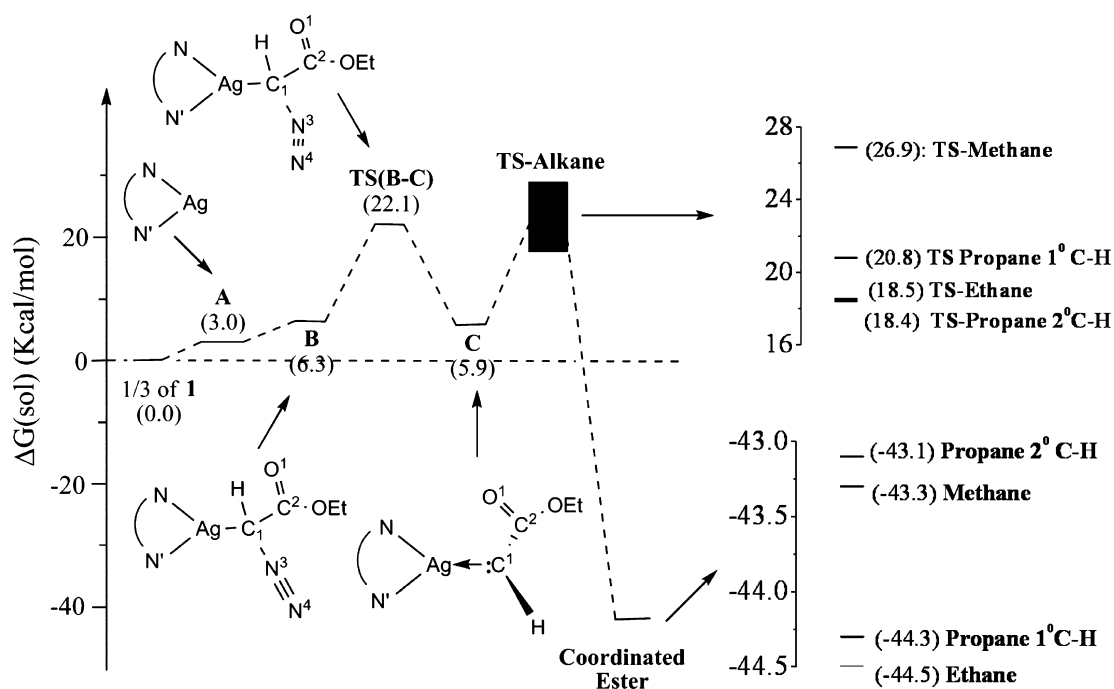


Figure 5. Computed reaction coordinate using complex **1** and various gaseous alkanes, such as methane, ethane, and propane. The transition states for initial formation of **1** and **B** cannot be located on the electronic surface, as these are dominated by the translational entropy change.

but in contrast, our system uses lower pressures of ethane in CH_2Cl_2 solvent.¹⁶ Unfortunately, many attempts to generate ethyl propanoate from methane activation and carbene insertion have so far eluded us, despite varying pressure, temperature, and solvent.

To examine the selectivity in C–H insertion chemistry, we also explored some branched alkanes given the presence of 1–3° carbons in these type of substrates (Table 5). Accordingly, 2-methylbutane yielded the ester-substituted products with greater selectivity in the 3° C–H position (insertion A, 8–24%), over the secondary and primary sites (insertions B and C, respectively). Likewise, using 2,3-dimethylbutane favored insertion of carbene into the 3° over the 1° position: A different regioselectivity was observed in the Dias's and Perez's groups using TpAg -based catalysts.^{20,21,23,24,29,31,38} The use of the C_6F_6 slightly improved the yield of the product and reduced the amount of unreacted EDA (entries 3, 4, 7, and 8; see Table 5).

Experimental and Theoretical Studies of the Reaction Mechanism. The Perez group has pioneered the copper- and silver-catalyzed insertion of the carbene fragment of $\text{N}_2\text{CH}(\text{CO}_2\text{Et})$ into alkane C–H bonds, primarily with trispyrazolylborate-ligated monovalent metal complexes.^{16,21,23,24} An evaluation of the mechanism, beginning from a preformed $\text{TpMCH}(\text{CO}_2\text{Et})$ carbene complex assumed to be an intermediate, has identified a transition state geometry in which the alkane never interacts with the metal and in which the C–H bond directly attacks the carbene carbon; the alkane approaches with the C–H vector nearly linearly pointed to the carbene carbon.⁷⁸ From their DFT studies, there is no significant interaction at the transition state (TS) of the alkane carbon with the carbene carbon, so the TS more resembles a hydrogen transfer process; C/C bond formation occurs much later than the TS.

This brings up the question of the charge character of the transferring hydrogen as well as whether the alkyl group is, in fact, captured in a concerted mechanism or whether a distinct

alkyl fragment (with whatever charge) in a geminate pair is, indeed, a participant. In the present study, we have ourselves discovered an analog of this catalysis, but with a *bidentate* ligand on silver(I). This carbene is anticipated to be electrophilic because silver is a poor π -base and it is an acceptor-substituted carbene.⁸ The lower coordination number at the metal raises the possibility of the empty metal orbital becoming involved, which is yet another mechanistic feature of this functionalization that we seek to understand: Is the mechanism here a small variant of the TpM -based catalysis, or do new mechanistic scenarios apply with our pyridylpyrrolide ligand-based catalysts? Key questions include the electronic character of the metal-carbene carbon^{6,11,12,15,23,24} and, indeed, the nature of the metal carbene bond for these metals, which are poor π -donors. Likewise, it would be important to appreciate the role, if any, that the metal has in the subsequent insertion event into the C–H bond.

Shown in Figure 5 is the computed pathway leading to carbene insertion into the C–H bond in methane, ethane, and propane.⁷⁴ Although we did not activate methane in the present study, we include these calculations to help us understand why this alkane is particularly difficult to activate and functionalize to the ester. As expected, all three reaction coordinates are comparable, with the only obvious variation being the C–H insertion transition state geometry. Surprisingly, the thermodynamic driving forces for coordinated product resulting from C–H insertion, $\text{Ag}(3,5\text{-}(\text{CF}_3)_2\text{PyrPy})(\text{ester})$ are quite similar and differ by no more than 1.4 kcal/mol. We wanted our computational analysis to clarify formation of the carbene complex, a point not previously computationally modeled, so we begin with intact EDA. We are certain that trinuclear **1** does not unimolecularly dissociate into monomers (based on VT ¹⁹F NMR spectra in pure alkane), so we anticipate that EDA attacks the trinuclear cluster and forms the complex $\text{Ag}(3,5\text{-}(\text{CF}_3)_2\text{PyrPy})(\text{EDA})$ (experiments support the formation of an

adduct), so we begin our mechanism from that species, since the barrier to formation of this adduct is expected to be low.

Complex $(3,5-(\text{CF}_3)_2\text{PyrPy})\text{Ag}[\text{CH}(\text{N}_2)\text{CO}_2\text{Et}]$ (**B**),⁷⁴ binds as a zwitterion through the diazonium carbon (since this intermediate is a precursor to N_2 elimination), with this carbon now tetrahedral, hence, a carbanion with a lone pair to share with silver. Intermediate **B** lies only 6.3 kcal/mol above the trinuclear species **1**. Our computed profile shows the loss of N_2 from **B** to be a concerted process and to involve a 22.1 kcal/mol barrier en route to the carbene $(3,5-(\text{CF}_3)_2\text{PyrPy})\text{Ag}(\text{CHCO}_2\text{Et})$ (**C**), which is nearly isothermal to **B** (5.9 kcal/mol; see Figure 5). The calculated $\text{Ag}-\text{C}$ distance in $(\text{EtCO}_2\text{CH})\text{Ag}(3,5-(\text{CF}_3)_2\text{PyrPy})$ is 2.01 Å, which is similar to distances from silver to *N*-heterocyclic carbene ligands,^{79–82} indicative of single bond character, thus rendering this carbene carbon, $\text{Ag}(\text{I})\leftarrow\text{C}(\text{CO}_2\text{Et})$, electrophilic (Figure 6). Shown

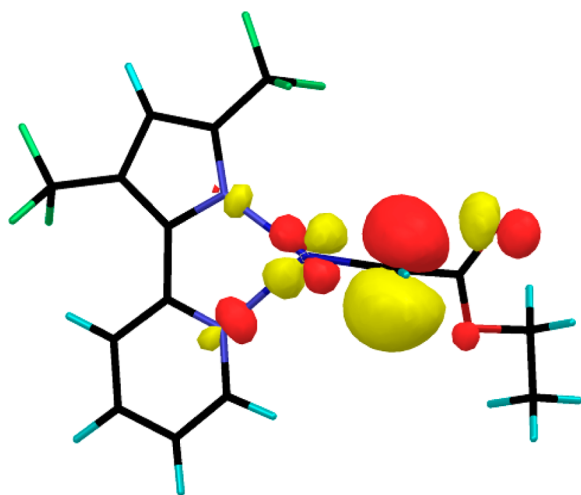


Figure 6. LUMO of $\text{Ag}(\text{I})\leftarrow\text{C}(\text{CO}_2\text{Et})$ showing carbene carbon participation in complex **C**.

in Figure 6 is the LUMO of putative **C** depicting the out-of-phase combination of the $\text{C } p_\pi$ orbital with the $\text{Ag } d_\pi$ orbital. The large contribution of the carbon empty *p* orbital therefore renders this system electrophilic where binding of the substrate exclusively interacts with the α -C. This carbene carbon LUMO character has also been used to explain the reactivity of halo-substituted carbenes coordinated to the $\text{Rh}_2(\text{O}_2\text{CR})_4$ moiety.⁸³

In an attempt to spectroscopically detect the elusive carbene complex, $(\text{EtCO}_2\text{CH})\text{Ag}(3,5-(\text{CF}_3)_2\text{PyrPy})$ (**C**), formed simply from **1** and EDA, these were combined (1:3 mol ratio) in CD_2Cl_2 at low temperatures. A ~ 0.05 M solution of **1** at -50 °C shows a color change from yellow to red after 30 min, and NMR spectra (^1H and ^{19}F) show 33% conversion to one new compound. We therefore conclude that EDA can effect, at most, partial conversion of catalyst precursor onto the catalytic cycle. Does this new compound contain intact diazoalkane, or has nitrogen already been evolved? To answer this, we combined **1** with EDA (1:3 mol ratio) for 30 min at -50 °C to form the equilibrium mixture of adduct and reagents. All volatiles were then removed first at -50 °C and then at 25 °C, fresh CD_2Cl_2 was added, and NMR spectra were recorded. These showed complete reforming to trinuclear complex **1** by both ^{19}F and ^1H NMR spectroscopy. This experiment rules out a nitrogen-loss carbene as the equilibrium participant (adduct identity) and is consistent with the **B/C** energy profile, which shows N_2 loss to have a significant barrier, possibly being

overall rate-determining. This spectroscopically observed species is proposed to be **B** or a linkage isomer adduct form involving the fragment $\text{Ag}(3,5-(\text{CF}_3)_2\text{PyrPy})$ and EDA.

Can theory also explain why methane is more difficult to activate than ethane? The TS for methane C–H insertion is at least ~ 6 kcal/mol higher in energy than the insertion of propane (Figure 5). In addition, judged by C/H bond length changes at the TS (TS-Alkane),⁷⁴ methane C–H insertion is earlier than the TS for ethane and other alkanes (Figure 7). Therefore, the challenge of methane activation is kinetic more than thermodynamic. In fact, insertion of carbene into the C–H bond of methane is overall rate-determining (26.9 kcal/mol), in contrast to propane and ethane, for which the RDS is loss of N_2 from species **B**. Careful inspection of the transition state geometries involving carbene insertion into the C–H bond of the alkane suggest a nonmetal-mediated H-atom transfer to be involved in the activation process (Figure 7), with the C/C distance being still nonbonding (angle C–H–C $\sim 130^\circ$). We believe some of these differences in energy barriers can be explained by the charge flow from the substrate to the electrophilic carbene. What is more remarkable is that analysis of charge flow by three different charge methods (ESP, Mulliken or NPA) all show that the change from separated reagents to the TS involves (Figure 8, $E = \text{CO}_2\text{Et}$) charge flow to the carbene carbon that is highlighted in green (hence it was an electrophilic center) from the arriving alkyl carbon, which is highlighted in blue (and not from the hydrogen from the incoming alkane, which is highlighted in yellow).

Shown in Figure 8 are the changes in NPA charges of the carbene carbon in intermediate **C** and the alkane C–H, when these combine to form the TS leading to the product of C–H insertion. These show methane and the 2° C–H group of propane for comparison purposes, and such NPA values clearly illustrate charge gain at the carbene carbon, no change at the migrating hydrogen, and loss of charge from the alkane carbon being activated. In both cases, the bridging H is best regarded as a conduit for charge flow in our proposed reaction mechanism.⁷⁴ As noted in Figure 7, we have found that as the C–H bond in C3 elongates with changing alkane, it places this carbon farther away from the carbene carbon, a contrast to the TS for methane activation. The process of C–H insertion is best described as asynchronous, in which there is some C–H formation at the carbene carbon with little C–C forming; thus, an early transition state with respect to product formation. For comparison, the transition state for addition of a secondary C–H bond (in cyclopentane) to the carbene $\text{C}(\text{Ph})(\text{CO}_2\text{Me})$ attached to a higher coordinate rhodium in $\text{Rh}_2(\text{O}_2\text{CH})_4$ has an even longer C/C separation, 2.409 Å.⁸⁴

Computational studies have identified that the transition state structure leading to methane activation contains a less obtuse $\text{C}_{\text{carbene}}\cdots\text{H}\cdots\text{CH}_3$ angle (C1–H1–C3 angle, 125.1°) than that observed for ethane (131.0°) and 2° C–H of propane (136.3°). Figure 7 depicts computed TS structures for the methane, ethane, and propane (the 2° C–H position is lower in energy by 2.4 kcal/mol than the 1° position, both of which are depicted) attack on $(\text{EtO}_2\text{CH})\text{Ag}(3,5-(\text{CF}_3)_2\text{PyrPy})$.⁷⁴ All substrates form thermodynamically stable products, but it is electronic factors that govern the kinetic preference for ethane and propane activation over methane insertion chemistry. Thus, although this selectivity correlates with lower energies of C–H homolysis for 2° and 3° C–H bonds, the real origin is better charge flow from *substituents* on the 2° and 3° C–H groups.

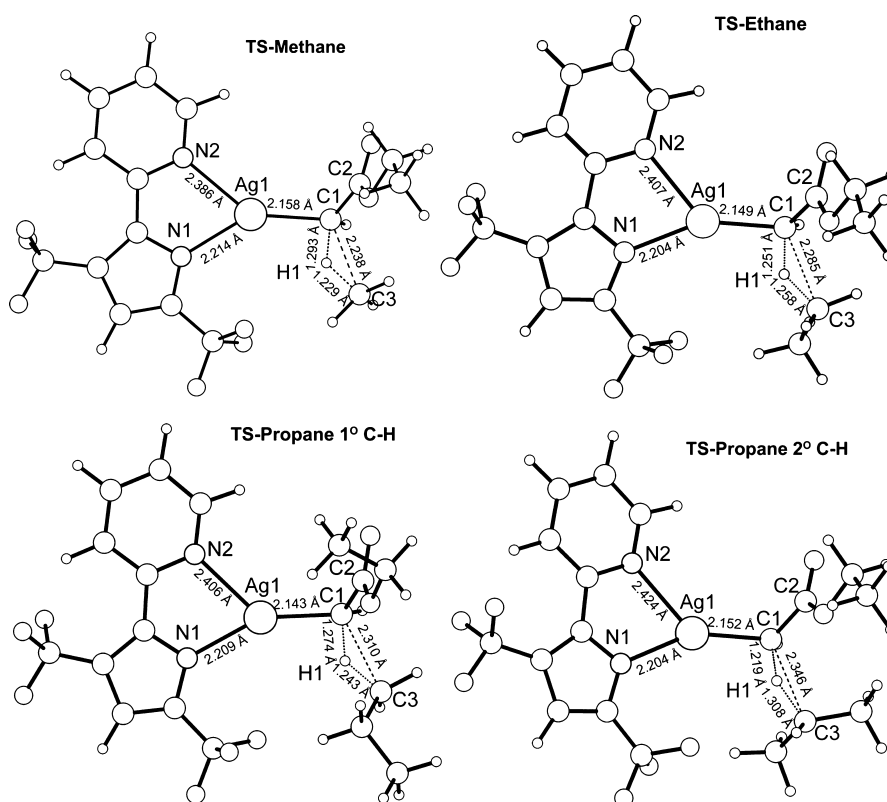


Figure 7. The transition states leading to the C–H insertion product are depicted, including the 1° and 2° C–H positions for propane.

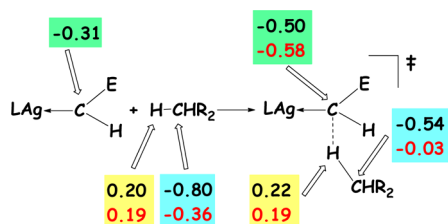


Figure 8. NPA charges for specific sites in carbene complex C (green for carbene carbon), the free alkane (yellow for hydrogen, blue for carbon), and the transition state leading to the C–H insertion product. Black font corresponds to CH₄, and red represents those for the 2° C–H position of propane.

Our computed reaction coordinate suggests the N₂ elimination step to be slow relative to carbene insertion in the C–H bond, with methane being the only exception because of the negative $\Delta\Delta G^\ddagger$ (ΔG^\ddagger for TS(B–C) – ΔG^\ddagger for TS-alkane).⁸⁵ Despite this, however, all $\Delta\Delta G^\ddagger$ are relatively small (–4.8 kcal/mol for methane, 3.6 kcal/mol for ethane, 1.3 for propane at the 1° carbon, and 3.7 kcal/mol for propane at the 2° carbon), suggesting these steps have similar activation energies.

To ascertain if C–H insertion is the slowest step in the reaction coordinate, we conducted a series of KIE experiments. Accordingly, a 1:1 cyclohexane/cyclohexane-*d*₁₂ internal competition and a catalytic amount of **1** with EDA revealed only a small KIE of 1.32(2) (based on integration of the two ester isotopologues), and irrespective of solvent (CD₂Cl₂ versus C₆F₆).^{85–87} Consequently, these data suggest that the product-determining step involves only modest C–H bond lengthening, which can also be represented as a very early transition state with respect to C–H insertion of the carbene. Our KIE value's

being close to unity (but not being 1) also demonstrates the C–H insertion step comes after the RDS in the case of cyclohexane. Our KIE value is much lower than Noel's, Wang's, as well as Adams's KIE reported for Rh₂(II,II) lantern systems inserting carbene from EDA into the C–H bond of cyclohexane,^{88,89} indicating an important mechanistic difference in our low-coordinate silver catalyst.

CONCLUSIONS

We report here results that collectively indicate that an alternative approach to cleavage of alkane C–H bonds is to create a very unsaturated metalcarbene, allowing a mechanism in which the alkane C–H bond never interacts with the metal, even when the complex we employ is unsaturated; this leads to addition of both R' and H to the carbene carbon, liberating a new sp³ hybridized carbon.

We have discovered an easy-to-prepare and -manipulate bidentate-coordinate silver system that exists in a trinuclear form, and that readily catalyzes, at 25 °C, the insertion of carbene from EDA into aliphatic C–H bonds of linear and branched hydrocarbons, as well as in ethane. Our computed reaction profile suggests a bent, two-coordinate silver fragment supports a carbene sufficiently electrophilic to react with alkane C–H bonds, and where N₂ extrusion is rate-determining for functionalization of ethane and propane. Our KIE near unity using cyclohexane as the substrate corroborates this theoretical prediction; however, the $\Delta\Delta G^\ddagger$ between the N₂ evolution step and the C–H insertion step decreases significantly when moving from propane to ethane to methane, to the point that C–H insertion into methane becomes overall rate-determining, despite all three products' being thermodynamically favorable. We propose that some of the selectivity for 2° vs 1° C–H insertion arises from substrate substituent-assisted charge flow

from the alkane carbon to the electrophilic carbene. Although an especially electrophilic metal (e.g., group 10) and electrophilic carbene substituent are clearly desirable to create a carbene sufficiently reactive to insert into alkane C–H bonds, recent work¹⁶ and that reported here show that additional “tuning” can be accomplished by heavily halogenating, especially fluorinating, the ancillary ligand. It is clear that our bidentate ligand, leaving silver unsaturated, assists this goal vs a tridentate tris-pyrazolylborate ligand. Being able to control the site of C–H insertion has become an active endeavor, since this approach can lead to direct functionalization of naturally occurring substrates as well as provide access to important natural products.^{90,91}

■ ASSOCIATED CONTENT

■ Supporting Information

Tables for C–H insertion reaction, computational information, spectral data, and information on the X-ray crystal structure analysis of compounds **1** (CIF file). This material is available free of charge via the Internet at <http://pubs.acs.org>.

■ AUTHOR INFORMATION

Corresponding Author

*E-mails: (D.J.M.) mindiola@indiana.edu, (K.G.C.) caulton@indiana.edu.

Notes

The authors declare no competing financial interest.

■ ACKNOWLEDGMENTS

We thank Indiana University Bloomington (FRSP) for financial support of this research. The authors acknowledge Dr. Jonathan A. Karty for assistance obtaining mass spectra. N.K. acknowledges support from JSPS Institutional Program for Young Researcher Overseas Visits.

■ REFERENCES

- (1) Demonceau, A.; Noels, A. F.; Hubert, A. J.; Teyssie, P. J. *Chem. Soc., Chem. Commun.* **1981**, 688–689.
- (2) Burgess, K.; Lim, H.-J.; Porte, A. M.; Sulikowski, G. A. *Angew. Chem., Int. Ed. Engl.* **1996**, *35*, 220–222.
- (3) Dias, H. V. R.; Browning, R. G.; Richey, S. A.; Lovely, C. J. *Organometallics* **2004**, *23*, 1200–1202.
- (4) Scott, L. T.; DeCicco, G. J. *J. Am. Chem. Soc.* **1974**, *96*, 322–323.
- (5) Davies, H. M. L. *J. Mol. Catal. A: Chem.* **2002**, *189*, 125–135.
- (6) Davies, H. M. L. *Angew. Chem., Int. Ed.* **2006**, *45*, 6422–6425.
- (7) Davies, H. M. L.; Antoulinakos, E. G. *J. Organomet. Chem.* **2001**, *617–618*, 47–55.
- (8) Davies, H. M. L.; Beckwith, R. E. J. *Chem. Rev.* **2003**, *103*, 2861–2903.
- (9) Davies, H. M. L.; Dick, A. R. *Top. Curr. Chem.* **2010**, *292*, 303–345.
- (10) Davies, H. M. L.; Hansen, T.; Churchill, M. R. *J. Am. Chem. Soc.* **2000**, *122*, 3063–3070.
- (11) Davies, H. M. L.; Manning, J. R. *Nature* **2008**, *451*, 417–424.
- (12) Davies, H. M. L.; Morton, D. *Chem. Soc. Rev.* **2011**, *40*, 1857–1869.
- (13) Doyle, M. P. *J. Org. Chem.* **2006**, *71*, 9253–9260.
- (14) Doyle, M. P.; Duffy, R.; Ratnikov, M.; Zhou, L. *Chem. Rev.* **2010**, *110*, 704–724.
- (15) Doyle, M. P.; McKervey, M.; Ye, T. *Modern Catalytic Methods for Organic Synthesis with Diazo Compounds: From Cyclopropanes to Ylides*; Wiley: New York, 1998.
- (16) Caballero, A.; Despagnet-Ayoub, E.; Diaz-Requejo, M. M.; Diaz-Rodriguez, A.; Gonzalez-Nunez, M. E.; Mello, R.; Munoz, B. K.; Ojo,

W.-S.; Asensio, G.; Etienne, M.; Perez, P. J. *Science* **2011**, *332*, 835–838.

(17) Caballero, A.; Diaz-Requejo, M. M.; Belderrain, T. R.; Nicasio, M. C.; Trofimenko, S.; Perez, P. J. *J. Am. Chem. Soc.* **2003**, *125*, 1446–1447.

(18) Caballero, A.; Diaz-Requejo, M. M.; Belderrain, T. R.; Nicasio, M. C.; Trofimenko, S.; Perez, P. J. *Organometallics* **2003**, *22*, 4145–4150.

(19) Caballero, A.; Diaz-Requejo, M. M.; Trofimenko, S.; Belderrain, T. R.; Perez, P. J. *Eur. J. Inorg. Chem.* **2007**, 2848–2852.

(20) Despagnet-Ayoub, E.; Jacob, K.; Vendier, L.; Etienne, M.; Alvarez, E.; Caballero, A.; Diaz-Requejo, M. M.; Perez, P. J. *Organometallics* **2008**, *27*, 4779–4787.

(21) Dias, H. V. R.; Lovely, C. J. *Chem. Rev.* **2008**, *108*, 3223–3238.

(22) Diaz-Requejo, M. M.; Belderrain, T. R.; Nicasio, M. C.; Trofimenko, S.; Perez, P. J. *J. Am. Chem. Soc.* **2002**, *124*, 896–897.

(23) Diaz-Requejo, M. M.; Perez, P. J. *J. Organomet. Chem.* **2005**, *690*, 5441–5450.

(24) Diaz-Requejo, M. M.; Perez, P. J. *Chem. Rev.* **2008**, *108*, 3379–3394.

(25) Fructos, M. R.; Belderrain, T. R.; de Fremont, P.; Scott, N. M.; Nolan, S. P.; Diaz-Requejo, M. M.; Perez, P. J. *Angew. Chem., Int. Ed.* **2005**, *44*, 5284–5288.

(26) Fuentes, M. A.; Rodriguez-Castillo, M.; Monge, M.; Olmos, M. E.; Lopez-de-Luzuriaga, J. M.; Caballero, A.; Perez, P. J. *Inorg. Chim. Acta* **2011**, *369*, 146–149.

(27) Lovely, C. J.; Flores, J. A.; Meng, X.; Dias, H. V. R. *Synlett* **2009**, 129–132.

(28) Morilla, M. E.; Diaz-Requejo, M. M.; Belderrain, T. R.; Nicasio, M. C.; Trofimenko, S.; Perez, P. J. *Organometallics* **2004**, *23*, 293–295.

(29) Rangan, K.; Fianchini, M.; Singh, S.; Rasika Dias, H. V. *Inorg. Chim. Acta* **2009**, *362*, 4347–4352.

(30) Rivilla, L.; Gomez-Emeterio, B. P.; Fructos, M. R.; Diaz-Requejo, M. M.; Perez, P. J. *Organometallics* **2011**, *30*, 2855–2860.

(31) Urbano, J.; Belderrain, T. R.; Nicasio, M. C.; Trofimenko, S.; Diaz-Requejo, M. M.; Perez, P. J. *Organometallics* **2005**, *24*, 1528–1532.

(32) Zakko, S. F.; Scirica, J. C.; Guttermuth, M. C.; Dodge, J.; Hajjar, J.-J. *Gastroenterology* **1997**, *113*, 232–237.

(33) Agboola, O. M.; Nwulu, N. I.; Egelioglu, F.; Agboola, O. P. *Int. J. Thermal Environ. Eng.* **2011**, *2*, 69–74.

(34) Solov'yanov, A. A. *Russ. J. Gen. Chem.* **2011**, *81*, 2531–2541.

(35) Liaquat, M.; Apenten, R. K. O. *J. Food Sci.* **2000**, *65*, 295–299.

(36) Xu, Y.; Wang, D.; Mu, X. Q.; Zhao, G. A.; Zhang, K. C. *J. Mol. Catal. B: Enzym.* **2002**, *18*, 29–37.

(37) Delgado-Rebollo, M.; Beltran, A.; Prieto, A.; Mar Diaz-Requejo, M.; Echavarren, A. M.; Perez, P. J. *Eur. J. Inorg. Chem.* **2012**, *2012*, 1380–1386.

(38) Dias, H. V. R.; Browning, R. G.; Richey, S. A.; Lovely, C. J. *Organometallics* **2005**, *24*, 5784.

(39) Diaz-Requejo, M. M.; Belderrain, T. R.; Nicasio, M. C.; Perez, P. J. *Dalton Trans.* **2006**, 5559–5566.

(40) Fructos, M. R.; De Fremont, P.; Nolan, S. P.; Mar Dauiaz-Requejo, M.; Perez, P. J. *Organometallics* **2006**, *25*, 2237–2241.

(41) Perez, J.; Morales, D.; Garcia-Escudero, L. A.; Martinez-Garcia, H.; Miguel, D.; Bernad, P. *Dalton Trans.* **2009**, 375–382.

(42) Rodriguez, P.; Alvarez, E.; Nicasio, M. C.; Perez, P. J. *Organometallics* **2007**, *26*, 6661–6668.

(43) Andino, J. G.; Flores, J. A.; Karty, J. A.; Massa, J. P.; Park, H.; Tsvetkov, N. P.; Wolfe, R. J.; Caulton, K. G. *Inorg. Chem.* **2010**, *49*, 7626–7628.

(44) Martin, C.; Munoz-Molina, J. M.; Locati, A.; Alvarez, E.; Maseras, F.; Belderrain, T. R.; Perez, P. J. *Organometallics* **2010**, *29*, 3481–3489.

(45) Urbano, J.; Braga, A. A. C.; Maseras, F.; Alvarez, E.; Diaz-Requejo, M. M.; Perez, P. J. *Organometallics* **2009**, *28*, 5968–5981.

(46) Pucci, D.; Aiello, I.; Aprea, A.; Bellusci, A.; Crispini, A.; Ghedini, M. *Chem. Commun.* **2009**, 1550–1552.

- (47) SAINT, *current version*; Bruker Analytical X-Ray Systems, Madison, WI.
- (48) Blessing, R. H. *Acta Crystallogr.* **1995**, *A51*, 33–38.
- (49) Burla, M. C.; Caliandro, R.; Carnalli, M.; Carrozzini, B.; Cascarano, G. L.; De Caro, O. L.; Giacovazzo, C.; Polidori, G.; Sagna, R. *Sir2004, A Program for Automatic Solution and Refinement of Crystal Structures, Version 1.0*; 2004.
- (50) Sheldrick, G. M. *Acta Crystallogr.* **2008**, *A64*, 112–122.
- (51) *Jaguar 7.7*, Schrödinger, LLC: New York, NY, 2007.
- (52) Becke, A. D. *Phys. Rev. A* **1988**, *38*, 3098–3100.
- (53) Becke, A. D. *J. Chem. Phys.* **1993**, *98*, 5648–5652.
- (54) Lee, C.; Yang, W.; Parr, R. G. *Phys. Rev. B: Condens. Matter* **1988**, *37*, 785–789.
- (55) Vosko, S. H.; Wilk, L.; Nusair, M. *Can. J. Phys.* **1980**, *58*, 1200–1211.
- (56) Hay, P. J.; Wadt, W. R. *J. Chem. Phys.* **1985**, *82*, 270–283.
- (57) Wadt, W. R.; Hay, P. J. *J. Chem. Phys.* **1985**, *82*, 284–298.
- (58) Dunning, T. H., Jr. *J. Chem. Phys.* **1989**, *90*, 1007–1023.
- (59) Edinger, S. R.; Cortis, C.; Shenkin, P. S.; Friesner, R. A. *J. Phys. Chem. B* **1997**, *101*, 1190–1197.
- (60) Friedrichs, M.; Zhou, R.; Edinger, S. R.; Friesner, R. A. *J. Phys. Chem. B* **1999**, *103*, 3057–3061.
- (61) Marten, B.; Kim, K.; Cortis, C.; Friesner, R. A.; Murphy, R. B.; Ringnalda, M. N.; Sitkoff, D.; Honig, B. *J. Phys. Chem.* **1996**, *100*, 11775–11788.
- (62) Halgren, T. A.; Lipscomb, W. N. *Chem. Phys. Lett.* **1977**, *49*, 225–232.
- (63) Peng, C.; Schlegel, H. B. *Isr. J. Chem.* **1993**, *33*, 449–454.
- (64) Flores, J. A.; Andino, J. G.; Tsvetkov, N. P.; Pink, M.; Wolfe, R. J.; Head, A. R.; Lichtenberger, D. L.; Massa, J.; Caulton, K. G. *Inorg. Chem.* **2011**, *50*, 8121–8131.
- (65) Catalano, V. J.; Malwitz, M. A. *Inorg. Chem.* **2003**, *42*, 5483–5485.
- (66) Catalano, V. J.; Munro, L. B.; Strasser, C. E.; Samin, A. F. *Inorg. Chem.* **2011**, *50*, 8465–8476.
- (67) Dias, H. V. R.; Diyabalanage, H. V. K. *Polyhedron* **2006**, *25*, 1655–1661.
- (68) Dias, H. V. R.; Gamage, C. S. P.; Keltner, J.; Diyabalanage, H. V. K.; Omari, I.; Eyobo, Y.; Dias, N. R.; Roehr, N.; McKinney, L.; Poth, T. *Inorg. Chem.* **2007**, *46*, 2979–2987.
- (69) Dias, H. V. R.; Palehpetiya Gamage, C. S. *Angew. Chem., Int. Ed.* **2007**, *46*, 2192–2194.
- (70) Dias, H. V. R.; Polach, S. A.; Wang, Z. *J. Fluorine Chem.* **2000**, *103*, 163–169.
- (71) Dias, H. V. R.; Singh, S.; Campana, C. F. *Inorg. Chem.* **2008**, *47*, 3943–3945.
- (72) Johnson, A. L.; Willcocks, A. M.; Richards, S. P. *Inorg. Chem.* **2009**, *48*, 8613–8622.
- (73) Zhang, X.; Gu, S.; Xia, Q.; Chen, W. *J. Organomet. Chem.* **2009**, *694*, 2359–2367.
- (74) See the Supporting Information.
- (75) Dias, H. V. R.; Browning, R. G.; Polach, S. A.; Diyabalanage, H. V. K.; Lovely, C. J. *J. Am. Chem. Soc.* **2003**, *125*, 9270–9271.
- (76) Paulissen, R.; Reimlinger, H.; Hayez, E.; Hubert, A. J.; Teyssie, P. *Tetrahedron Lett.* **1973**, *14*, 2233–2236.
- (77) Wurz, R. P.; Charette, A. B. *Org. Lett.* **2002**, *4*, 4531–4533.
- (78) Braga, A. A. C.; Maseras, F.; Urbano, J.; Caballero, A.; Mar Diaz-Requejo, M.; Perez, P. J. *Organometallics* **2006**, *25*, 5292–5300.
- (79) Arduengo, A. J., III; Dias, H. V. R.; Calabrese, J. C.; Davidson, F. *Organometallics* **1993**, *12*, 3405–3409.
- (80) Guerret, O.; Sole, S.; Gornitzka, H.; Teichert, M.; Trinquier, G.; Bertrand, G. *J. Am. Chem. Soc.* **1997**, *119*, 6668–6669.
- (81) Hu, X.; Tang, Y.; Gantzel, P.; Meyer, K. *Organometallics* **2003**, *22*, 612–614.
- (82) Liu, Q.-X.; Yao, Z.-Q.; Zhao, X.-J.; Chen, A.-H.; Yang, X.-Q.; Liu, S.-W.; Wang, X.-G. *Organometallics* **2011**, *30*, 3732–3739.
- (83) Bonge, H. T.; Hansen, T. *J. Org. Chem.* **2010**, *75*, 2309–2320.
- (84) Hansen, J.; Autschbach, J.; Davies, H., M. L. *J. Org. Chem.* **2009**, *74*, 6555–6563.
- (85) Nakamura, E.; Yoshikai, N.; Yamanaka, M. *J. Am. Chem. Soc.* **2002**, *124*, 7181–7192.
- (86) Bonge, H. T.; Hansen, T. *Eur. J. Org. Chem.* **2010**, 4355–4359.
- (87) Gomez-Gallego, M.; Sierra, M. A. *Chem. Rev.* **2011**, *111*, 4857–4963.
- (88) Demonceau, A.; Noels, A. F.; Costa, J. L. *J. Mol. Catal.* **1990**, *58*, 21–26.
- (89) Wang, P.; Adams, J. *J. Am. Chem. Soc.* **1994**, *116*, 3296–3305.
- (90) Newhouse, T.; Baran, P. S. *Angew. Chem., Int. Ed.* **2011**, *50*, 3362–3374.
- (91) White, C. M. *Science* **2012**, *335*, 807–809.